Redox Biology 22 (2019) 101156

Contents lists available at ScienceDirect

Redox Biology

journal homepage: www.elsevier.com/locate/redox

Research Paper

Age-related oxidative stress confines damage-responsive Bmi1^{+} cells to perivascular regions in the murine adult heart

Diego Herrero[a,1], Susana Cañón[a,1], Guillermo Albericio[a], Rosa María Carmona[a], Susana Aguilar[a], Santos Mañes[b], Antonio Bernad[a,*]

[a] Cardiac Stem Cells Group, Department of Immunology and Oncology, National Center for Biotechnology (CNB-CSIC), 28049, Madrid, Spain
[b] Signaling Networks in Inflammation and Cancer Group, Department of Immunology and Oncology, National Center for Biotechnology (CNB-CSIC), 28049, Madrid, Spain

ARTICLE INFO

Keywords:
Bmi1
Damage-responsive cell
Vasculature
Oxidative damage
Reactive oxygen species

ABSTRACT

Adult progenitor cells reside in specialized microenvironments which maintain their undifferentiated cell state and trigger regenerative responses following injury. Although these environments are well described in several tissues, the cellular components that comprise the cardiac environment where progenitor cells are located remain unknown. Here we use Bmi1^{CreERT} and Bmi1^{GFP} mice as genetic tools to trace cardiac damage-responsive cells throughout the mouse lifespan. In adolescent mice, Bmi1^{+} damage-responsive cells are broadly distributed throughout the myocardium. In adult mice, however, Bmi1^{+} cells are confined predominately in perivascular areas with low levels of reactive oxygen species (ROS) and their number decline in an age-dependent manner. *In vitro* co-culture experiments with endothelial cells supported a regulatory role of the endothelium in damage-responsive cell behavior. Accordingly, *in vivo* genetic decrease of ROS levels in adult heart disengaged Bmi1^{+} cells from the cardiovascular network, recapitulating an adolescent-like *Bmi1* expression profile. Thus, we identify cardiac perivascular regions as low-stress microenvironments that favor the maintenance of adult damage-responsive cells.

1. Introduction

Several studies report that adult mammals generate new mature cardiac cells although with a cell lineage-specific rate [1–3]. *De novo* cardiomyogenesis is limited to ≈1% per year, in fact, most cardiomyocytes are never exchanged [1]. The cellular source of endogenous cardiomyocyte renewal continues to be debated; several studies report a very low contribution to *de novo* cardiomyocytes from previously described c-Kit^{+} (0.03% per year) and Sca1^{+} (0.014% per year) adult cardiac progenitor cells [4–6]. The proliferation of mature cardiomyocytes accounts around 0.6% of *de novo* cardiomyocytes per year [7,8], however, typically experimental proofs of cardiomyocyte division (Ki-67, PCNA [proliferating-cell-nuclear-antigen], PHH3 [phosphorylated histone H3] and Aurora-B-Kinase staining) could be overestimating this percentage [9]. Unlike cardiomyogenesis, cardiac endothelial and mesenchymal cells (including fibroblasts and stromal cells) are highly proliferative, with estimates ranging from 5% to 20% per year [1,5]. Several studies show that adult cardiac progenitor cells contribute actively to cardiac myofibroblasts and endothelial cells [10–16]. These cardiac progenitor cells respond to cardiac injury contributing to the, clearly limited, regenerative process [10,11,17,18]. The set of all these lineage-specific cardiac progenitors (cardiomyocyte-, endothelial-, myofibroblast-progenitors) will be generically denoted hereafter as damage-responsive cells (DR-cells).

Polycomb repressive complex 1, containing a BMI1 core component, regulates mitochondrial function [19] and cellular senescence through repression of the INK4a locus [20]. Accordingly, high BMI1 expression is widely linked to the regenerative capacity of adult tissues and identifies cells with progenitor-related characteristics [21–24]. In cardiac cells, recent reports indicate that BMI1 represses differentiation to cardiomyocyte through direct interactions with regulatory regions of cardiogenic genes [25,26]. In the adult heart, high BMI1 expression distinguishes a mixture of endothelial- and mesenchymal-related Sca1^{+} cells able to contribute *in vivo* to the three main cardiac lineages [27,28]. More importantly, these cells are necessary for injury-induced angiogenesis and for the physiological cardiac remodeling after myocardial infarction [12], thus identifying a population of cardiac DR-cells.

* Corresponding author. Department of Immunology & Oncology, National Center for Biotechnology (CNB-CSIC), Campus de Cantoblanco de la Universidad Autónoma de Madrid, E-28049, Madrid, Spain.
E-mail address: abernad@cnb.csic.es (A. Bernad).
[1] D.H. and S.C. contributed equally to this study.

https://doi.org/10.1016/j.redox.2019.101156
Received 14 January 2019; Received in revised form 23 February 2019; Accepted 27 February 2019
Available online 04 March 2019

Knowledge of adult progenitor cell populations and stem cell therapy have improved with the identification of their niches, such as epithelial crypts and perivascular niches [29]. Adult stem cell niches are neither homogeneous nor static throughout the life of the mouse. In bone marrow, different niches regulate lineage-biased hematopoietic stem cells [30]. In addition, the aging of bone marrow-, neural- and muscle-niches reduce the regenerative potential of hematopoietic stem cells, neural stem cells and satellite cells, respectively [31–33]. In the adult heart, however, the identity and characteristics of the microenvironment sustaining cardiac DR-cells remains unknown. In this report we assess the location of cardiac DR-cells and their evolution with aging.

2. Methods

2.1. Transgenic mice and tamoxifen administration

Transgenic mice used in this study were Bmi1$^{CreERT/+}$, Bmi1$^{GFP/+}$, Rosa26$^{mT.mG/+}$, Rosa26$^{Tomato/+}$ (All from The Jackson Laboratory), Gli1$^{CreERT/+}$ [10], G6PD^{Tg} [34] and Sod3$^{-/-}$ [35], and all were on the C57BL/6 background. Tamoxifen (Tx; Sigma, T5648) was dissolved in corn oil (Sigma, C8267) and intraperitoneally (i.p.) injected (103 μg/g body weight). Experiments were carried out in male and female mice as recommended by the US National Institutes of Health since preliminary analysis revealed no differences between males and females [36]. 7-8-week-old mice were used as adult mice unless otherwise indicated in the text. Animal studies were approved by the CNB-CSIC ethics committee and by the Division of Animal Protection of the Comunidad de Madrid (PA 56/11, PROEX 048/16). All animal procedures conformed to EU Directive 2010/63EU and Recommendation 2007/526/EC regarding the protection of animals used for experimental and other scientific purposes, enforced in Spanish law under Real Decreto 1201/2005.

2.2. Isolation of adult mouse cardiomyocytes and non-myocyte cells

Non-myocyte cells and cardiomyocytes were obtained by the Langendorff method using retrograde perfusion through the aorta. The heart was removed rapidly and retrograde-perfused under constant pressure (60 mmHg; 37 °C, 8 min) in Ca^{2+}-free buffer (113 mM NaCl, 4.7 mM KCl, 1.2 mM $MgSO_4$, 5.5 mM glucose, 0.6 mM KH_2PO_4, 0.6 mM Na_2HPO_4, 12 mM $NaHCO_3$, 10 mM $KHCO_3$, 10 mM Hepes, 10 mM 2,3-butanedione monoxime, and 30 mM taurine). Digestion was initiated by adding a mixture of recombinant enzymes (0.2 mg/ml Liberase Blendzyme (Roche, 05401127001), 0.14 mg/ml trypsin (ThermoFisher, 15090046), and 12.5 μM $CaCl_2$) to the perfusion solution. When the heart became swollen (10 min), it was removed and gently teased into small pieces with fine forceps in the same enzyme solution. Heart tissue was further dissociated mechanically using 2, 1.5, and 1 mm-diameter pipettes until all large heart tissue pieces were dispersed. The digestion buffer was neutralized with stopping buffer (10% fetal bovine serum (FBS; Capricorn, FBS-12A), 12.5 μM $CaCl_2$). Cardiomyocytes were pelleted by gravity (7 times, 30 min each), and the supernatant was used as a source of non-myocyte cardiac cells [27].

2.3. Acute myocardial infarction

Mice were anesthetized with 4% sevoflurane, intubated, and ventilated with a 50% air:oxygen mixture using a positive-pressure respirator (Minivent 845, Harvard; 160 strokes/min, 250 μl tidal volume). A left thoracotomy was performed via the fourth intercostal space and the lungs were retracted to expose the heart. After opening the pericardium, the left anterior descending coronary artery was ligated with 7-0 silk suture approximately 2 mm below the edge of the left atrial appendage. Ligation was considered successful when the anterior wall of the left ventricle turned pale. The lungs were inflated by increasing positive end-expiratory pressure and the thoracotomy site was closed in layers with 6-0 suture. Mice were maintained on a 37 °C heating pad until recovery and for 2 h after surgery. The control mouse group underwent sham ligation, with a similar surgical procedure but without tightening the suture around the coronary artery.

2.4. Vascular permeability and Evans blue dye assay

Adult mice (20 g body weight) received histamine (2.5 mg; Sigma, H7125) in phosphate-buffered saline (PBS) via intravenous (i.v.) injection. Hearts were harvested 36 h later and digested by the Langendorff method.

For the Evans blue (EB) dye assay, 4 h after histamine injection mice received 100 μl of 0.5% EB (Sigma, E2129) in PBS via i.v. injection. Mice were euthanized 30 min later and hearts were perfused with 10 ml of PBS through the left ventricle to remove excess EB from vessels. Hearts were then desiccated (24 h, 60 °C), followed by EB dye elution in formamide (Millipore, 109684; 24 h, 65 °C). To analyze the amount of EB in the supernatant, samples were placed in a 96-well plate and read with a Multiskan GO Spectrophotometer (Thermo Scientific) at 620 and 720 nm, correcting for contaminating heme pigments: A_{620} (EB) = A_{620}-(1.426 × A_{720} + 0.030) [37]. The EB concentration was calculated against a standard curve.

2.5. In vivo EdU proliferation assay

5-ethynyl-2′-deoxyuridine (EdU; Sigma, T511285) was dissolved in 0.9% NaCl and stored at 10 mg/ml. For proliferation experiments, mice received EdU (10 μg/g, i.p., once daily, as indicated in the figure legends). Hearts were digested by the Langendorff method or frozen for histology. Proliferating cells were detected with *Click-iT Imaging* (C10640) or *Click-iT Flow Cytometry* (C10634) kits (ThermoFisher) following the manufacturer's protocol.

2.6. In vivo reactive oxygen species (ROS) measurement

To detect ROS *in vivo*, adult mice (20 g body weight) received CellROX (100 μl, 2 mM, i.v., ThermoFisher, C10422) diluted in 0.9% NaCl just before use. Mice were euthanized 2 h later and hearts were perfused with 10 ml of PBS through the left ventricle to remove excess CellROX. Hearts were immediately frozen in OCT compound (Tissue-Tek, 25608-930), sectioned at 8-μm intervals on a cryostat, briefly fixed in 4% paraformaldehyde (PFA, TED PELLA, 18505; 5 min at room temperature (RT)), and permeabilized (0.1% PBS-Triton X-100 (Sigma, X100); 10 min, RT). Preparations were incubated with primary endothelial antibodies (Table S2) and processed normally (see Immunohistochemical analyses). CellROX images were captured with a Zeiss LSM 700 confocal microscope with fixed settings and pseudocolor assignment was based on fluorescence intensity (Fiji v2.0.0, 2015; NIH). Using 12-bit images (color level range 0–4095), putative non-stained areas (0–50) were discarded and ROS^{low} areas (50–800) were distinguished from ROS^{high} areas (> 800). Intensity threshold between high versus low ROS areas was defined with heart sections from 24 h paraquat-treated mice (ROSgenic product [38]; 20 mg/kg, Sigma, 36541). Paraquat-treated hearts showed > 50% heart surface with > 800 intensity level. For histological quantification of ROS levels, at least 30 representative transverse heart sections from complete ventricles were used ($n \geq 5$).

2.7. Immunohistochemical analyses and computational modeling of Bmi1^{+} cell localization

Hearts were fixed in 4% PFA overnight at 4 °C and cryopreserved in 30% saccharose, frozen in OCT compound, and sectioned at 8-μm intervals on a cryostat. Briefly, sections were washed in PBS and incubated with permeabilization buffer (0.1% Triton X-100; 20 min, RT).

Slides were rinsed in blocking buffer (5% bovine serum albumin, Sigma, A7906; 1 h, RT) and incubated with primary (Table S2; overnight; 4 °C) and secondary (1 h, RT) antibodies, incubated with DAPI (Sigma, D9542; 20 min, RT) and mounted with ProLong antifade reagent (ThermoFisher, P36930) as we previously described [27].

Computational simulation of randomly distributed Bmi1$^+$ cardiac cells was done using Tile Scan files of series of images from 8-μm transversal heart sections. Only ventricle sections were selected for development of computational modeling due to the structural differences between ventricles and atria. To simulate a random cell distribution model avoiding experimental bias, we used the same Tile Scan images used to measure observed Euclidean distances. The number of randomly placed Bmi1$^+$ cells was selected based on the number of observed Bmi1$^+$ cells detected in each individual heart section. Because the hearts of Bmi1$^{CreERT/+}$Rosa26$^{Tomato/+}$G6PD^{Tg} mice and Bmi1$^{CreERT/+}$Rosa26$^{Tomato/+}$ mice are equal in size, an increase in the number of Bmi1$^+$ cells in the former would increase the probability that they are found closer to endothelium structures. The set of all simulations defined a two-dimensional cell distribution that we would observe for non-preferentially localized Bmi1$^+$ cells in relation to the respective structures. Computational simulation and measurement of the distances were performed in a blind manner by two researchers. If the *in situ* Euclidean distance measurements were not-statistically different from those obtained by a random placement of Bmi1$^+$ cells, this would indicate a non-preferential spatial distribution. The computational simulation was performed using ImageJ software (Fiji v2.0.0).

For histological quantification of the two-dimensional distance from Bmi1$^+$ cells to the respective structures, at least 30 representative transverse heart sections from ventricles were used ($n \geq 3$). Images were captured with a Zeiss LSM 700 confocal microscope. Processing, including pseudocolor assignment and changes in brightness, was applied uniformly to the entire image to equalize the appearance of multiple panels in a single figure.

2.8. In vitro cell culture

Primary Sca1$^+$Bmi1$^+$CD45$^-$ and PDGFRα$^+$ mesenchymal-like cells were sorted after Langendorff digestion and expanded in Iscove's modified Dulbecco's medium (IMDM, ThermoFisher, 12440053) containing 10% FBS, 100 IU/ml penicillin, 100 mg/ml streptomycin and 2 mM L-glutamine (all from Invitrogen), 10^3 units ESGRO Supplement (Millipore, ESG1106), 10 ng/ml EGF (epidermal growth factor; Sigma, SRP3196) and 20 ng/ml FGF (fibroblast growth factor; Peprotech, 100-18B) (37 °C, 3% O_2, 5% CO_2). Primary adult cardiac endothelial cells (CD31$^+$) were obtained with the Neonatal Cardiac Endothelial Cell Isolation Kit (Miltenyi, 130-104-183). CD31$^+$ primary cells and the 1g11 endothelial cell line [39] were expanded in VascuLife VEGF Endothelial Medium Complete Kit (Lifeline Cell Technology, LL-0003) (37 °C, 21% O_2, 5% CO_2). Primary cardiac cells were used for the experiments at passage ≤9.

2.9. Co-culture experiments

Endothelial/mesenchymal-like cells were seeded at 4×10^4 cells/cm^2 on 0.1% gelatin-treated plates. Cells were washed with PBS 8 h later, and cardiac DR-cells were seeded at the same density directly onto the endothelial/mesenchymal cell monolayers in Sca1$^+$Bmi1$^+$CD45$^-$ cell culture medium. All analyses were done after 12 h of co-culture in Bmi1$^+$ cardiac DR-cell culture medium (37 °C, 21% O_2, 5% CO_2).

To label actively proliferating cells, EdU (10 μM) was added to the co-culture 12 h prior to analysis and proliferating cells were detected with the *Click-iT Imaging* kit (ThermoFisher).

Total ROS (CellROX) and mitochondrial mass (MitoTracker Green, M7514; both ThermoFisher) were used following the manufacturer's protocols. In all experiments, Bmi1$^+$ cardiac DR-cells were detected based on intrinsic Tomato (cells isolated from Bmi1$^{CreERT/+}$R26$^{Tomato/+}$ mice) or GFP (from Bmi1$^{GFP/+}$ mice) fluorescence.

2.10. Recombinant protein assays

For EphrinB2 or EphB4 stimulation, clustered EphrinB2-Fc or EphB4-Fc (both from R&D Systems, 496-EB and 446-B4; 5 μg/ml) were absorbed on 0.1% gelatin-coated cell culture plates (2 h, 37 °C). Clustering was achieved using anti-human IgG, Fcγ fragment specific antibody (Jackson ImmunoResearch, 109-005-098) at a 2:1 M ratio, as described [40]. After 12 h, cells were detached from dishes and GFP fluorescence was measured by FACS.

For the Fc protein binding assay, Bmi1$^+$ DR-cells were detached from dishes, washed twice (5% FBS/PBS) and incubated with 2 μg/ml Fc-fusion proteins (1 h, 4 °C). After washing, cells were incubated with PE-conjugated goat anti-human IgG(H + L) (Jackson ImmunoResearch, 109-116-088; 1 h, 4 °C). Stained cells were analyzed with a FACSGallios instrument (Becton Dickinson).

For VEGFA stimulation, VEGFA (R&D Systems, 493-MV; 10 ng/ml) was added to Bmi1$^+$ cardiac DR-cell cultures for 12 h prior to analysis.

2.11. Flow cytometry

For flow cytometry analysis, hearts were digested by the Langendorff method and cell- or cardiomyocyte-enriched fractions analyzed. In total, > 10000 events were collected for each sample and gates were set manually using negative controls. Cell sorters used were Beckman Coulter Moflow XDP and BD FacsAria II Special Order System, and cell cytometers were Beckman Coulter GALLIOS Analyzer and BD FACSCanto II. Kaluza v1.5 was used for data analysis.

2.12. Western blotting

For western blotting, cells and tissues were lysed (45 min, 4 °C) in radioimmunoprecipitation assay buffer (RIPA; Sigma-Aldrich, R0278), with addition of cOmplete, EDTA-free Protease Inhibitor Cocktail (Roche, 04-693-132-001). Proteins were quantified using a Multiskan GO Spectrophotometer (Thermo Scientific). Lysates were size-fractionated by SDS-polyacrylamide gel electrophoresis, transferred to Hybond ECL nitrocellulose membranes (ThermoFisher, IB401002), probed with indicated antibodies (Table S2) and analyzed by enhanced chemiluminescence (GE Healthcare, RPN2209).

2.13. RT-qPCR analysis

RNA was purified using the Cells-to-CT Kit (Ambion, ThermoFisher, 4402953). Complementary DNA was obtained by reverse transcription with the High Capacity cDNA Reverse Transcription Kit (Applied Biosystems, 4368814). cDNAs were analyzed by real-time PCR using the Power SYBR Green PCR Master Mix (Applied Biosystems, 4367659). Amplification, detection and data analysis were carried out with an ABI PRISM 7900HT Sequence Detection System and normalized to *GusB* and *Gapdh* expression. Changes in mRNA expression are noted as ×-fold change relative to the control. qPCR primers are listed in Table S2.

2.14. RNA-Seq and accession numbers

Methods for RNA isolation and sequencing of freshly sorted CD45$^-$Sca1$^+$Bmi1$^+$ *vs.* CD45$^-$Sca1$^+$Bmi1$^-$ cardiac cells have been described in detail elsewhere [17]. The GEO accession number for RNA-Seq data reported is GSE55754.

2.15. Statistical analysis

Statistical analyses were performed with GraphPad Prism 6.01. Data were subjected to the Shapiro-Wilk test for normality and F test for

equality of variances. For two groups, those that passed normality and equal variance tests were analyzed by Student's *t*-test (2-tailed, unpaired), and those that failed normality and equal variance tests were analyzed by the non-parametric Mann-Whitney Rank Sum test. Non-parametric two-sample Kolmogorov-Smirnov test was used to analyze cell distributions. For analysis of multiple groups, data that passed normality and equal variance tests were analyzed by one-way ANOVA with Tukey's post-hoc test, and those data that failed normality and equal variance tests were analyzed by the Kruskal-Wallis test with Dunn's multiple comparisons test. All experiments were reproduced at least three times with similar results. A value of $P < 0.05$ was considered significant, and $P > 0.05$ was labeled as n.s. (not significant). All replicates considered are biological replicates.

3. Results

3.1. Percentage and types of Bmi1$^+$ DR-cells decrease in an age-dependent manner

We traced damage-responsive (DR) cells in postnatal hearts using Bmi1$^{GFP/+}$ mice, in which green fluorescence protein (GFP) expression is driven by endogenous *Bmi1* regulatory elements [41]. The percentage of non-myocyte Bmi1$^+$ DR-cells decreased in an age-dependent manner from adolescence (2–3-weeks-old) to adulthood (4-months-old), and continued to decrease in geriatric mice (> 24-months-old) (Fig. 1A and B). In contrast to the decrease in the percentage of Bmi1$^+$ DR-cells, GFP intensity slightly increased in remaining adult Bmi1$^+$ DR-cells (Fig. 1C). These results show a decrease of Bmi1$^+$ DR-cells linked with heart aging.

To identify Bmi1$^+$ cells in heart sections we used tamoxifen (Tx)-inducible Bmi1$^{CreERT/+}$Rosa26$^{tdTomato/+}$ mice (denoted hereafter as Bmi1-cre^{Tomato}), since GFP signal in cryosections from Bmi1$^{GFP/+}$ mice was difficult to distinguish from background. Tomato expression 5 days post-Tx induction in Bmi1-cre^{Tomato} mice resembles GFP expression in Bmi1$^{GFP/+}$ mice [12] and the percentage of Tomato$^+$ cells was similar to that assessed by fluorescence-activated cell sorting (FACS), indicating that the immunohistochemistry analysis was robust (Fig. S1A). In adolescent mice 5 days post-Tx induction, *Bmi1* was expressed in various cell types, including mature lineages (Fig. 1D–G). In adult mice 5 days post-Tx induction, *Bmi1* expression was nonetheless restricted to non-myocyte Sca1$^+$ cells (Fig. 1D, F-H). In addition, and as observed in other organs, *Bmi1* deficiency led to higher levels in *p16^{INK4a}* and *p19^{ARF}* senescence-related genes in *Bmi1* haploinsufficient hearts (Bmi1$^{+/-}$) [41] than in wild-type hearts (Fig. 1I). Altogether, these results show an age-dependent reduction in the percentage of Bmi1$^+$ DR-cells and a restriction in the cardiac cell lineages that expresses BMI1 throughout mouse lifespan.

3.2. Bmi1$^+$ DR-cells display a perivascular gradient-like cell distribution in adult heart

Adult progenitor cells reside in microenvironments that maintain progenitor identity and control cell-fate decisions [42]. To identify the Bmi1-cell environment, we used confocal imaging to visualize heart sections from 5 days Tx-induced Bmi1-cre^{Tomato} adult mice. The majority of Bmi1$^+$ DR-cells were located in the left ventricle (≈70%), particularly in the lateral free wall; however, we detected the highest relative density in the right ventricle (Figs. S1B and C). In all cases, Bmi1$^+$ DR-cells were located in a gradient-like distribution around cardiac vasculature, but never in the tunica intima of blood vessels (Fig. 1H). To gain detailed insight into their location, we examined the spatial relationship between Bmi1$^+$ DR-cells and vasculature using two-dimensional tile scanning of heart sections. We found that more than half of total Bmi1$^+$ DR-cells were located within 60-μm of vasculature (Fig. 1J), preferentially close to small vessels but with no preference to coronary veins or arteries (Figs. S1D and E). We used computational simulations to statistically confirm such a biased cell distribution (see Methods and Fig. S1F for details). We verified that the observed Bmi1$^+$ DR-cell distribution was similar in all analyzed mice (Fig. S1G) and was significantly different to the expected distribution of randomly placed cells (grey bars in Fig. 1J). The spatial relationship between cardiac damage-responsive cells and vasculature was not restricted to Bmi1$^+$ DR-cells, as we statistically confirmed a similar relationship with proposed Gli1$^+$ myofibroblast progenitors [10] (Fig. S1H). In contrast to adult heart, Bmi1$^+$ DR-cells displayed a random cell distribution in adolescent hearts, suggesting that perivascular environment becomes relevant in an aging-dependent fashion (Fig. 1K).

3.3. Non-proliferating Bmi1$^+$ DR-cells are close to cardiac vasculature

As described in other adult stem cell niches, we hypothesized that cardiac vasculature might exert a regulatory role on Bmi1$^+$ DR-cells [43,44]. We evaluated their cell cycle status and distribution in relation to cardiac vasculature in steady state. Fourteen days after daily 5-ethynyl-2′-deoxyuridine (EdU) administration (Fig. 2A), we observed that the mean distance of EdU$^+$ Bmi1$^+$ DR-cells to endothelium was significantly different to that of EdU$^-$ cells (Fig. 2B). The largest percentage of EdU$^+$ Bmi1$^+$ DR-cells was located in a zone 40–60-μm to the nearest endothelium (50% of total Bmi1$^+$ DR-cells in 40–60-μm area) (Fig. 2B). Whereas the largest percentage of total Bmi1$^+$ DR-cells resided very close to the endothelium, only a small percentage of these cells (≈10% of total) were proliferating (20% of total Bmi1$^+$ DR-cells in 0 − 20-μm area) (Fig. 2B and C). To determine whether cardiac injury could alter the distribution of proliferating Bmi1$^+$ DR-cells, we performed a similar analysis after acute myocardial infarction (AMI) (Fig. 2D). We no longer detected a spatial relationship of proliferating Bmi1$^+$ DR-cells with the endothelium, suggesting extensive cell cycle entry (Fig. 2E). Despite the impairment of cardiac vasculature after AMI, we detected the largest percentage of EdU$^+$ Bmi1$^+$ DR-cells (≈30% of total) close to the vasculature (70% of total Bmi1$^+$ DR-cells in 0 − 20-μm zone) (Fig. 2E and F). Altogether, these results show that non-proliferating Bmi1$^+$ DR-cells are preferentially located close to the endothelium in homeostasis, but this cell distribution is no longer apparent after damage, when perivascular Bmi1$^+$ DR-cells proliferate intensely.

3.4. Endothelial cells regulate the behavior of Bmi1$^+$ DR-cells in vitro

Many of the endothelial-Bmi1$^+$ DR-cell interactions are challenging to study *in vivo*. We attempted to mimic these interactions by co-culturing primary Bmi1$^+$ cardiac DR-cells isolated from 5 days Tx-induced adult Bmi1-cre^{Tomato} mice [12] with the endothelial 1g11 cell line [39] and also with primary cardiac endothelial cells (CD31$^+$). Co-culture with primary mesenchymal cardiac cells (PDGFRα$^+$) was used as a control (Fig. S2A). We first examined Bmi1$^+$ DR-cell proliferation following an *in vitro* EdU pulse. We detected that only heterotypic culture with endothelial cells decreased cardiac Bmi1$^+$ DR-cell proliferation (Fig. 3A and B). In addition to cell cycle regulation, and as we expected based on reported niche properties [43,44], we observed that direct contact with endothelial cells also reduced total reactive oxygen species (ROS) levels in Bmi1$^+$ DR-cells, which was concomitant with a decrease in total mitochondrial mass (Fig. 3C and D). We then evaluated whether endothelial-Bmi1$^+$ DR-cell contact maintained Bmi1$^+$ cell identity by measuring *Bmi1* expression. We isolated Bmi1$^+$ DR-cells from Bmi1$^{GFP/+}$ mice (GFP$^+$) and co-cultured with membrane tomato cardiac endothelial cells from Rosa26$^{mT.mG/+}$ mice (mT$^+$) [45] (Fig. 3E). *Bmi1* expression was higher in co-cultured Bmi1$^+$ DR-cells than in those cultured alone (Fig. 3F).

Endothelial cells stimulate stem-like cells in normal and cancer tissues through both cell-cell contact and soluble factors [44,46]. We performed comparative RNA sequencing (RNA-Seq) analysis of Bmi1$^+$ *vs.* Bmi1$^-$ adult cardiac cells to identify potential endothelial-related

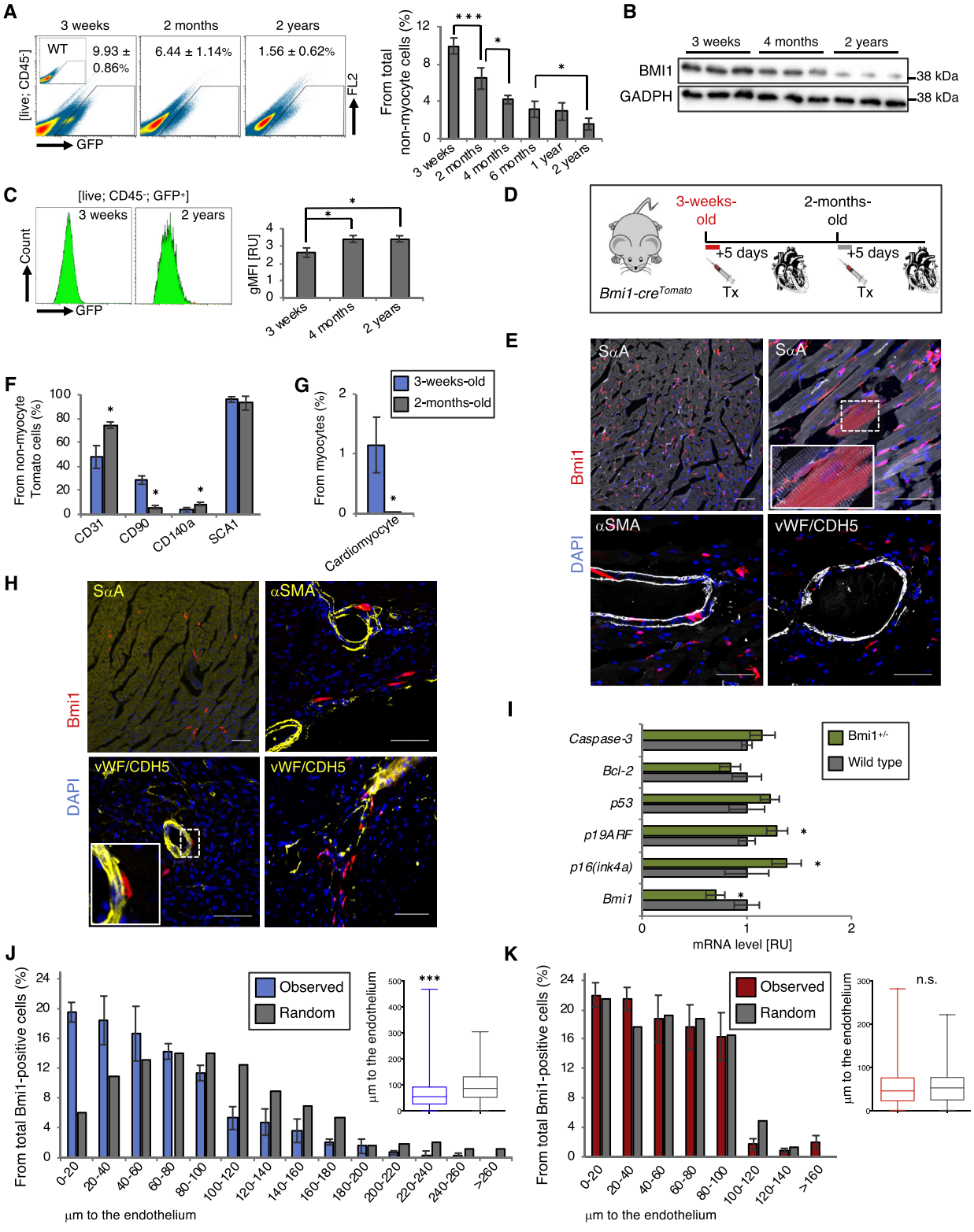

(caption on next page)

signaling pathways that could mediate the crosstalk with neighboring endothelial cells (Table S1). Heat map and fold change analyses showed that in Bmi1^{+} DR-cells both *EphrinB2/EphB4* and *Vegfa/Vegfr2* signaling pathways were potential candidates to mediate interactions with endothelial cells (Fig. 3G and H). As described in tumor cells [46], we found that VEGFA stimulation upregulated *Bmi1* expression in Bmi1^{+} DR-cells isolated from Bmi1$^{GFP/+}$ mice (Fig. 3I). EPHRINB2 and EPHB4 are preferentially expressed on arterial and venous cardiac endothelium, respectively [47]. Because *EphrinB2/EphB4* signaling is bi-directional, we examined the ability of recombinant EphrinB2-Fc and EphB4-Fc proteins to bind to Bmi1^{+} cardiac DR-cells. Both proteins bound to a fraction of Bmi1^{+} DR-cells (Fig. 3J) and activated *Bmi1*

Fig. 1. Age-associated decrease of perivascular cardiac Bmi1$^+$ DR-cells. **(A)** Representative FACS plots (left) and quantification (right) of non-myocyte cardiac cells from Bmi1$^{GFP/+}$ mice at indicated ages (n = 8). *Inset*, cardiac cells from wild-type mouse. **(B)** BMI1 expression in whole hearts from C57BL/6 mice at indicated ages analyzed by western blot. (n = 6) **(C)** Representative histograms (left) and quantification (right) of GFP geometric mean fluorescence intensity (gMFI) of cardiac GFP$^+$ cells isolated from Bmi1$^{GFP/+}$ mice at indicated ages (n = 8). **(D)** Timeline of Tx induction and heart analysis of adolescent (3-weeks-old) and adult (2-months-old) Bmi1-cre^{Tomato} mice. **(E)** Representative heart cryosections of 3-week-old Bmi1-cre^{Tomato} mice 5 days post-Tx induction. *Inset*, Bmi1$^+$ cardiomyocyte (2 × magnification). Cardiomyocyte (SαA), smooth muscle cell (αSMA), endothelial cell (vWF/CDH5). **(F & G)** Comparative FACS characterization of non-myocyte (f) and myocyte (g) cells from 3-week-old (blue) and 2-month-old (grey) Bmi1-cre^{Tomato} mice 5 days post-Tx induction (n = 4). **(H)** Representative heart cryosections of 2-month-old Bmi1-cre^{Tomato} mice 5 days post-Tx induction. *Inset*, perivascular Bmi1$^+$ cell (2 × magnification). **(I)** Bmi1-related genes in whole hearts from 2-month-old Bmi1$^{+/-}$ (green) and C57BL/6 (grey) mice, measured by RT-qPCR (n = 4). **(J & K)** Distribution of Bmi1$^+$ DR-cells in relation to coronary vasculature compared to cell distribution of randomly positioned Bmi1$^+$ cells on maps of heart sections in relation to the same cell structure (grey) in adult (J, blue) and adolescent (K, red) heart (n = 4; > 1000 Bmi1$^+$ cells/heart). *Insets*, box plot graph from the cell distribution. (a,c): *p < 0.05, ***p < 0.001; 1-way ANOVA with Tukey post-hoc test (f,g,i): *p < 0.05; Mann-Whitney rank-sum test (j,k): *p < 0.05, ***p < 0.001; 2-sample Kolmogorov-Smirnov test. RU, relative units; SαA, sarcomeric alpha actinin; vWF, von Willebrand Factor; CDH5, VE-cadherin; αSMA, alpha smooth muscle actin. Bars, 50 µm. Data shown as mean ± SEM.

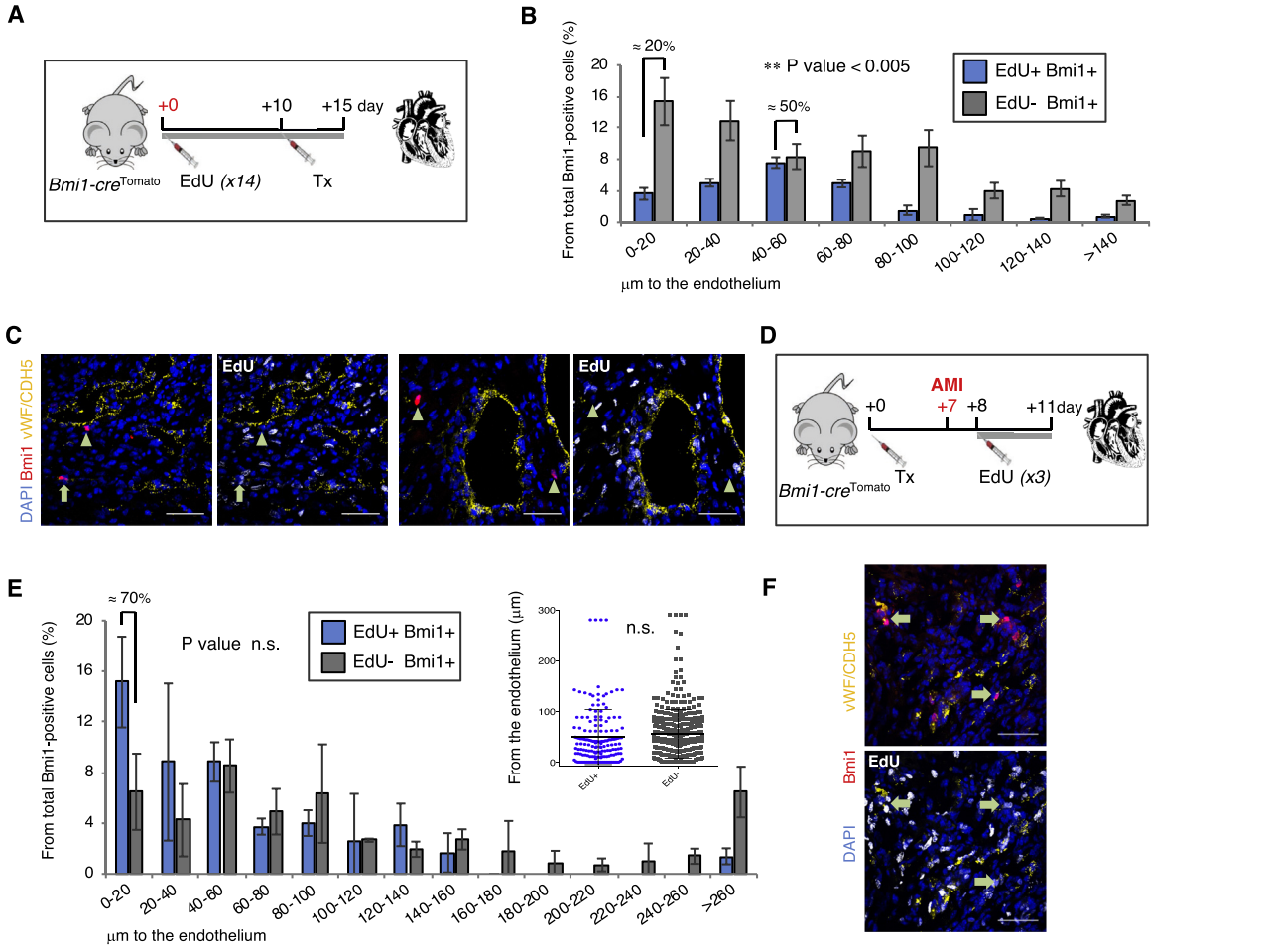

Fig. 2. Spatial relationship between proliferating Bmi1$^+$ DR-cells and cardiac vasculature in homeostasis and after injury. **(A)** Timeline of EdU labeling of *in vivo* proliferating Bmi1$^+$ cells from Bmi1-cre^{Tomato} mice in homeostasis. **(B)** Distribution of non-proliferating (EdU$^-$, grey) and proliferating (EdU$^+$, blue) Bmi1$^+$ cardiac DR-cells in relation to endothelium (n = 4; > 200 EdU$^+$Bmi1$^+$ and > 800 EdU$^-$Bmi1$^+$ cells/heart). **(C)** Representative heart cryosections of adult Bmi1-cre^{Tomato} mice 15 days after the beginning of EdU administration. Arrowheads, EdU$^-$Bmi1$^+$ cells; arrows, EdU$^+$Bmi1$^+$ cells. **(D)** Timeline of EdU labeling of *in vivo* proliferating Bmi1$^+$ cells from Bmi1-cre^{Tomato} mice after acute myocardial infarction (AMI). **(E)** Distribution of EdU$^+$ (blue) and EdU$^-$ (grey) Bmi1$^+$ cells in relation to endothelium 4 days after AMI (n = 4; > 400 EdU$^+$Bmi1$^+$ and > 800 EdU$^-$Bmi1$^+$ cells/heart). *Inset*, graph of mean distance. **(F)** Representative heart cryosection of adult Bmi1-cre^{Tomato} mice 4 days after AMI. Arrows, EdU$^+$Bmi1$^+$ cells. (b,e): *p < 0.05, **p < 0.005; 2-sample Kolmogorov-Smirnov test. Bars, 50 µm. Data shown as mean ± SEM.

expression (Fig. 3K), suggesting that Bmi1$^+$ cells comprise a mixture of artery- (EphB4$^+$) and venous-related (EphrinB2$^+$) perivascular cells. Altogether, our findings strongly suggest that Bmi1$^+$ DR-cell maintenance depends on the combinatorial regulation of several signaling pathways that depends on endothelial cells. From this network of signaling pathways, our data highlight EPHRINB2/EPHB4 and VEFGA/VEGFR2 signaling as potential mediators in the fine-tuning of endothelial-Bmi1$^+$ cardiac DR-cell interactions.

3.5. Cardiac Bmi1$^+$ DR-cells are sheltered in perivascular areas with low ROS levels

As Bmi1$^+$ cardiac DR-cells displayed a gradient-like distribution around cardiac vasculature rather than a discrete perivascular distribution, we reasoned that additional mechanisms could regulate Bmi1$^+$ cell distribution. We pharmacologically disrupted endothelial barrier function in Bmi1$^{GFP/+}$ mice by administration of histamine

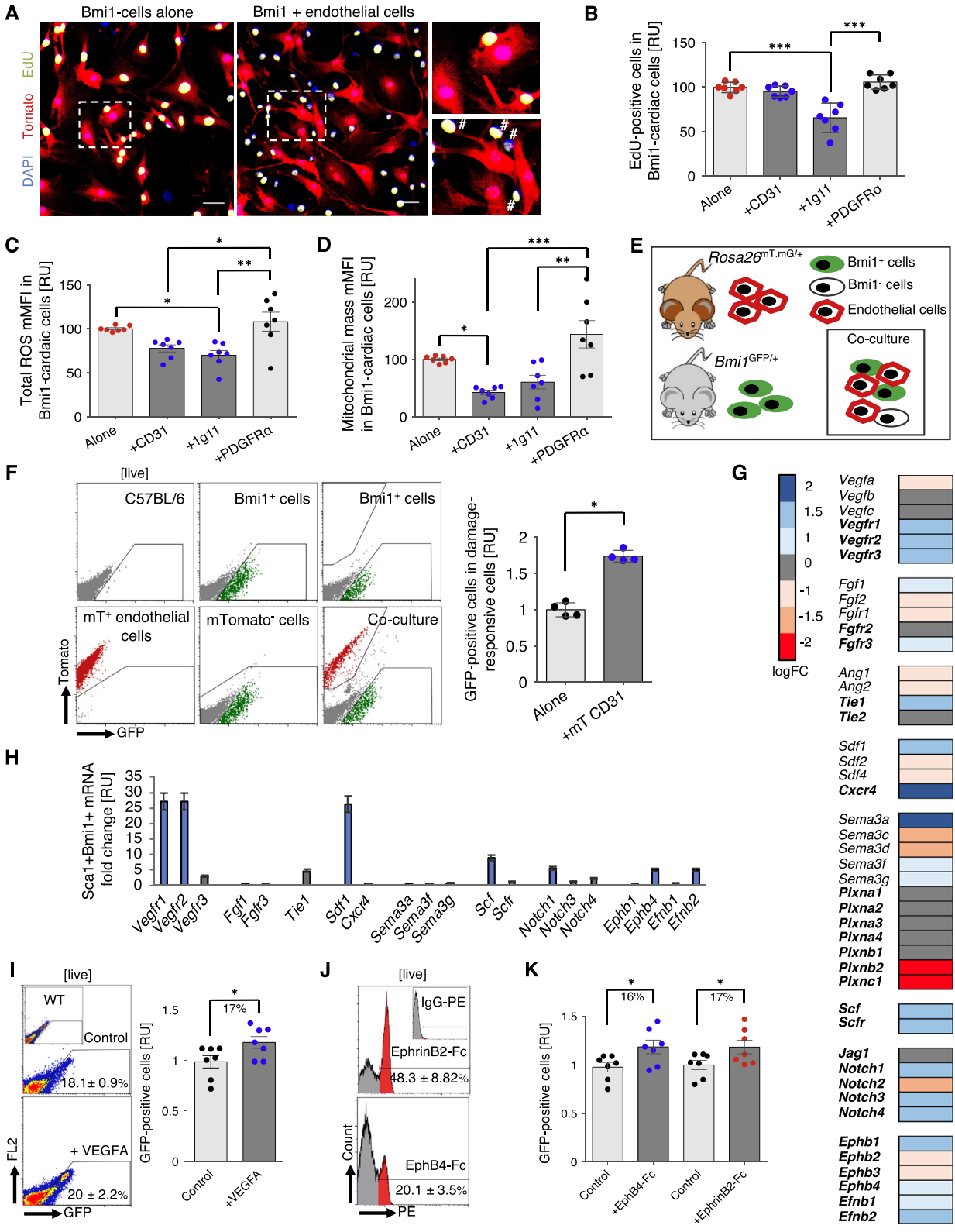

(caption on next page)

[37,48] (Figs. S2B and C). After histamine treatment, we observed a significant reduction in the percentage of perivascular Bmi1$^+$ DR-cells (Fig. 4A) that was not explained by an increase in Bmi1$^+$ cardiac cell death or *Bmi1* downregulation mediated by histamine (Fig. 4B and C). These results show that integrity of the vascular barrier is relevant for the maintenance of perivascular environment where cardiac damage-responsive cells are located.

Cardiac Bmi1$^+$ DR-cells display low levels of ROS *in vivo* and are resistant to oxidative damage [26]. To test whether the capacity of blood vessels to generate low-ROS areas in their proximity [43,49] contributes to shelter Bmi1$^+$ cells, we *in vivo* stained total ROS in hearts from Bmi1-cre^{Tomato} adult mice 5 days post-Tx induction (Fig. S2D).

Fig. 3. Instructive role of endothelial cells *in vitro* through both cell-cell contact and soluble factors. **(A)** Representative immunocytochemistry images of proliferating Bmi1$^+$ DR-cells cultured alone (left, Tomato cells) and co-cultured with endothelial cells (right, Tomato + endothelial cells). *Insets*, proliferating and no-proliferating Bmi1$^+$ cells in monoculture (top) and Bmi1$^+$ cells co-cultured with endothelial cells (bottom; # indicates endothelial cells) (2 × magnification). Bars, 50 μm. **(B)** EdU$^+$Bmi1$^+$ cells after *in vitro* mono- or co-culture with indicated cell types ($n = 7$). **(C & D)** Total ROS (c) and mitochondrial mass (d) mode fluorescence intensity (mMFI) of Bmi1$^+$ DR-cells after *in vitro* mono- or co-culture with indicated cell types, measured by FACS ($n = 7$). **(E)** Sorting strategy to isolate mTomato$^+$ cardiac endothelial cells (CD31$^+$) from Rosa26$^{mTmG/+}$ mice and Bmi1$^+$ cardiac DR-cells from Bmi1$^{GFP/+}$ mice. **(F)** Representative FACS plots (left) and quantification (right) of mono- or co-culture experiments of cardiac endothelial cells (mTomato$^+$) with Bmi1$^+$ cardiac DR-cells (GFP$^+$) isolated from Bmi1$^{GFP/+}$ mice ($n = 4$). **(G)** Heat map of endothelial-related genes enriched in CD45$^-$Sca1$^+$Bmi1$^+$ *vs.* CD45$^-$Sca1$^+$Bmi1$^-$ freshly sorted cells from adult hearts as measured by RNA-Seq. Genes in bold correspond to cell membrane molecules ($n = 3$). **(H)** RT-qPCR validation of RNA-Seq upregulated endothelial-related genes relative to *GusB/Gapdh* levels in CD45$^-$Sca1$^+$Bmi1$^+$ freshly sorted cardiac cells ($n = 3$). Blue bars indicate mRNA fold change expression ≥5. **(I)** Representative FACS plots (left) and quantification (right) of Bmi1$^+$ cell percentage after *in vitro* VEGFA or control treatment of cells isolated from Bmi1$^{GFP/+}$ mice ($n = 7$). *Inset*, Sca1$^+$ wild type (WT) cardiac cells *in vitro*. **(J)** EphrinB2-Fc (top) and EphB4-Fc (bottom) fusion proteins bind to a set of Bmi1$^+$ cardiac DR-cells *in vitro*. *Inset*, Bmi1$^+$ cells stained with PE-conjugated anti-human IgG alone ($n = 7$). **(K)** Percentage of Bmi1$^+$ cells (GFP) after *in vitro* stimulation with recombinant EphrinB2-Fc and EphB4-Fc proteins ($n = 7$). (b,c,d): *p < 0.05, **p < 0.005, ***p < 0.001; 1-way ANOVA with Tukey post-hoc test (f): *p < 0.05; Mann-Whitney rank-sum test (i, k): *p < 0.05; unpaired Student t-test. Data shown as mean ± SEM.

The total ROS staining detected the increase in cardiac ROS levels after paraquat treatment, confirming that the staining was robust (Fig. S2D). In addition to identifying perivascular zones with high ROS levels, we also found perivascular areas with very low levels of ROS (Fig. 4D) coinciding with the localization of the majority of Bmi1$^+$ DR-cells (Fig. 4E and F). Along with the decrease in the percentage of Bmi1$^+$ DR-cells in adult hearts (Fig. 1A), we detected and age-dependent increase in total ROS levels, without difference in perivascular areas (Fig. 4G). Overall, these results suggest that the ROS^{low} environment harbors Bmi1$^+$ cardiac DR-cells. Aging restricts the extension of these areas without affecting perivascular environment, thus maintaining the perivascular Bmi1$^+$ DR-cells in adulthood.

3.6. Reduction of ROS levels disengaged Bmi1$^+$ DR-cells from the vasculature

To confirm the importance of perivascular ROS, we genetically decreased ROS levels by crossing Bmi1$^{GFP/+}$ mice with glucose-6-phosphate dehydrogenase transgenic mice (G6PD^{Tg}), which boosts tissue protection from aging-associated functional decline (denoted hereafter as Young^{induced}) [34]. As a negative control, we crossed Bmi1$^{GFP/+}$ mice with superoxide dismutase 3 knockout mice (Sod3$^{-/-}$), in which endothelial-related *Sod3* deficiency increases vascular nitric oxide consumption and, therefore, displays features of accelerated aging (denoted hereafter as Aged^{induced}) [35] (Fig. 5A). Hearts were harvested from adolescent to adult mice to cover the temporal window during which the largest decrease of Bmi1$^+$ cardiac cells occurred (see Fig. 1A and B). The decrease in oxidative damage in Bmi1$^{GFP/+}$Young^{induced} mice (Figs. S3A and B) triggered an increase in the percentage of cardiac Bmi1$^+$ DR-cells in adolescent mice and delayed their age-associated loss (Fig. 5B and C). In agreement, the increase in oxidative damage in Bmi1$^{GFP/+}$Aged^{induced} mice (Figs. S3C and D) accelerated the age-related loss of cardiac Bmi1$^+$ DR-cells (Fig. 5D).

To gain more insight into the effect of G6PD overexpression in *Bmi1* expression profile, we analyzed histological heart sections of Bmi1-cre^{Tomato}Young^{Induced} adult mice 5 days post-Tx treatment. No differences in vascularization were detected between adolescent and adult Bmi1-cre^{Tomato} and adult Bmi1-cre^{Tomato}Young^{Induced} hearts (Fig. S3E). Included in the large number of Bmi1$^+$ cells in Bmi1-cre^{Tomato}Young^{Induced} hearts, we detected mature cardiac cell types such as smooth muscle, cardiomyocytes and mature endothelial cells (Fig. 5E). The *Bmi1* expression profile in Bmi1-cre^{Tomato}Young^{Induced} adult hearts from 5 days Tx-treated mice resembled that of Bmi1-cre^{Tomato} adolescent hearts from 5 days Tx-treated adolescent mice, suggesting an *in vivo* delay of the aged-dependent cell-lineage restriction of *Bmi1* expression (Fig. 5F, G and Fig. S4).

We then analyzed the distance of cardiac Bmi1$^+$ DR-cells to the nearest vasculature in 5 days post-Tx induced Bmi1-cre^{Tomato}Young^{Induced} adult mice (blue) and found no differences in the mean distance or cell distribution compared with the expected distribution of randomly placed cells (grey; Fig. 5H). These results show that the genetic decrease of ROS levels leads to *Bmi1* expression in cell types where *Bmi1* is not expressed in steady state. Accordingly, the genetic decrease of ROS levels in adult hearts altered the close spatial relationship of Bmi1$^+$ DR-cells with the cardiovascular network, resembling it to adolescent wild-type hearts.

4. Discussion

Several studies suggest that hypoxic zones, epicardium and the vasculature provide a protective microenvironment for damage-responsive cells in adult heart [10,50,51]. Although there is evidence that some damage-responsive cells have a perivascular localization [10,52], an in-depth analysis of cell distribution has not been undertaken to our knowledge. Here, our cell distribution analysis statistically confirmed the vasculature as a partner in the still undefined microenvironment for adult cardiac Bmi1$^+$ damage-responsive cells.

Cardiac vasculature is heterogeneous in developmental origin, cell composition and functional specialization [47]. As is the case for neural- and bone marrow-endothelium [43,44], our data strongly suggest an active role of cardiac vasculature in homeostasis and tissue repair; endothelial cells are able to *trans*-differentiate into cardiomyocytes, smooth muscle cells and myofibroblasts [52–54], and coronary vasculature is linked to progenitor cells both during development [55] and adulthood [6,10]. Moreover, cardiac endothelial cells have the highest exchange rate in the low cell turnover of the adult heart [1].

The study of cellular constituents of the vascular niche has emphasized its complexity in various tissues [56]. Most adult stem cells are located close to small-size arterioles [43,49] but not directly linked to hypoxic zones [49]. Although Bmi1$^+$ DR-cells are located close to small-size vessels, our results suggest that they are not preferentially located in artery or vein perivascular-areas. Blood vessels regulate adult progenitor identity through cell-cell contact [44], production of cytokines [43] or generation of zones with low ROS levels [49]. We showed that endothelial cell crosstalk with Bmi1$^+$ DR-cells was driven by both cell-cell contact and endothelial-related soluble factors. In addition, we found that the cell-type and the percentage of cells which express BMI1 were influenced by total ROS levels. Aging correlated with an increase in ROS levels in the myocardium, while in the adult heart endothelial network maintained low-ROS areas in its proximity that sheltered Bmi1$^+$ DR-cells.

The relationship between ROS and progenitor cell maintenance has been extensively studied. High ROS levels induce DNA damage, mitochondrial dysfunction and early aging [26,57]. Accordingly, the highest heart regeneration capacity is seen during embryo development, which occurs in an environment with low-ROS levels [57]. The postnatal ROS increase is linked to cell cycle exit of cardiomyocytes [57] and, in adulthood, high ROS levels activate the expression of a cardiogenic differentiation program [26,58]. It is therefore not unexpected that adult cardiac damage-responsive cells are nested and

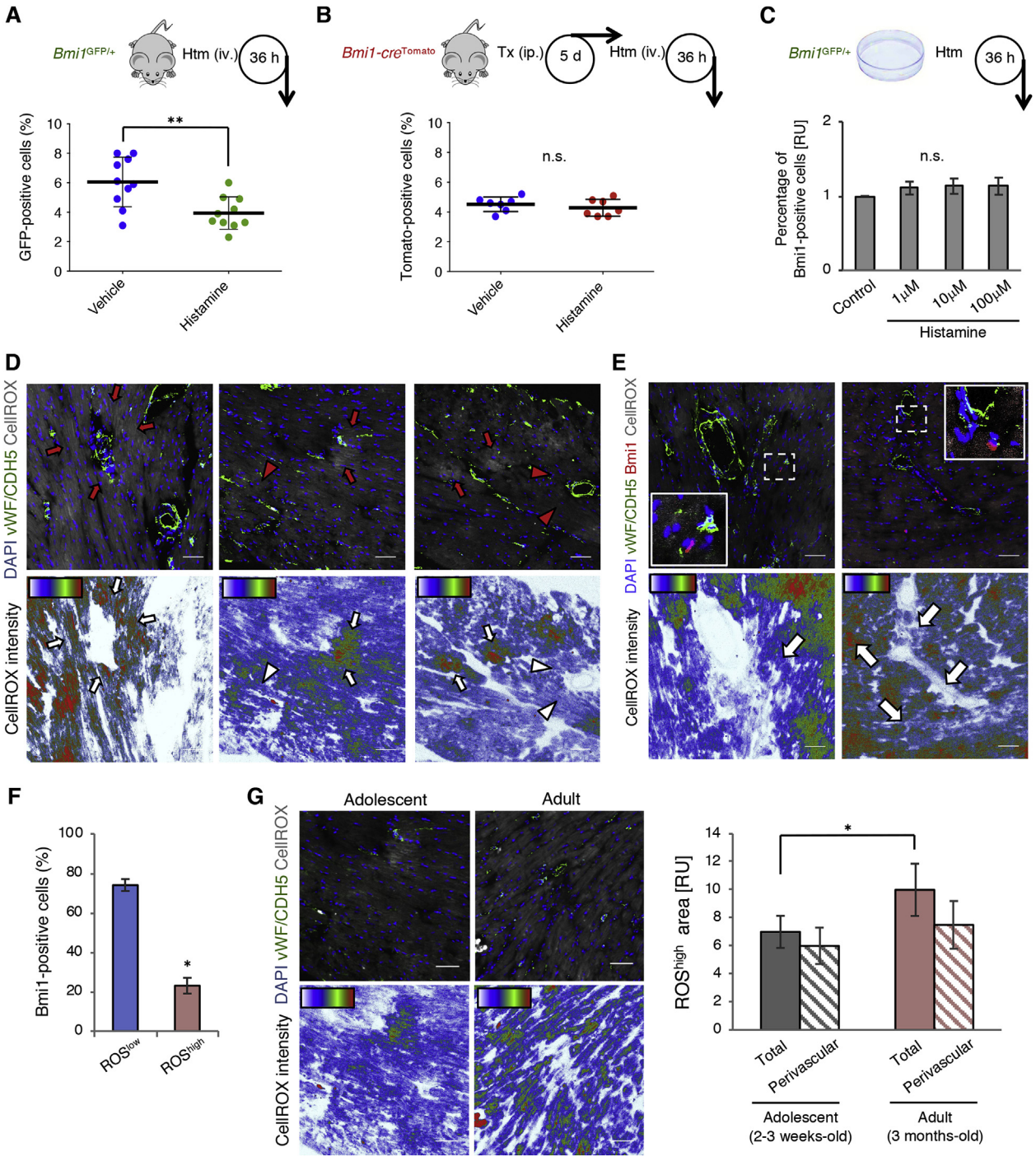

Fig. 4. Cardiac Bmi1$^+$ DR-cells are located in low-ROS microenvironments close to cardiac vasculature. **(A & B)** Percentage of Bmi1$^+$ cells after endothelial barrier disruption by histamine administration in Bmi1$^{GFP/+}$ mice (n = 10) (a) and in Bmi1-cre^{Tomato} Tx-induced mice (n = 7) (b), measured by FACS. **(C)** Percentage of GFP$^+$ cells from sorted and *in vitro* cultured Bmi1$^+$ cells from Bmi1$^{GFP/+}$ hearts after indicated histamine treatments *in vitro*, measured by FACS (n = 3). **(D)** Representative heart images (top) and CellROX pseudocolor assignment (bottom) of CellROX-stained heart sections from Bmi1-cre^{Tomato} mice. Arrows, perivascular high-ROS areas; arrowheads, perivascular low-ROS areas. **(E)** Representative *in vivo* CellROX-stained heart cryosections from Bmi1-cre^{Tomato} mice 5 days post-Tx induction. *Insets*, Bmi1$^+$ cells (5 × magnification). Arrows, Bmi1$^+$ cell position in pseudocolor CellROX intensity map. **(F)** Quantification of Bmi1$^+$ cell location in CellROX intensity map (n = 5; > 500 cells/heart). **(G)** Representative *in vivo* CellROX-stained heart cryosections (left) and quantification of CellROX intensity (right) from adolescent and adult Bmi1-cre^{Tomato} mice (n = 5). (a,b): **p < 0.005; unpaired Student t-test (c): n.s.; Kruskall-Wallis ANOVA test (f,g): *p < 0.05; Mann-Whitney rank-sum test. Htm, histamine. Bars, 50 μm. Data shown as mean ± SEM.

maintained in low-ROS areas, confirming oxidative stress as a limiting factor of cardiac regenerative capacity.

Aging is the result of the combination of genetically programmed events and extrinsic damages, although both events are closely connected. Ineffective ROS regulation is linked with the generation and progression of cardiac aging [59,60] and all suggested methods to delay cardiac aging such as caloric restriction [61], mitochondrial manipulation [62], pharmacological treatments [63] share the oxidative damage reduction effect. Here, we identify low ROS areas such as the microenvironment for cardiac damage-responsive cells. This

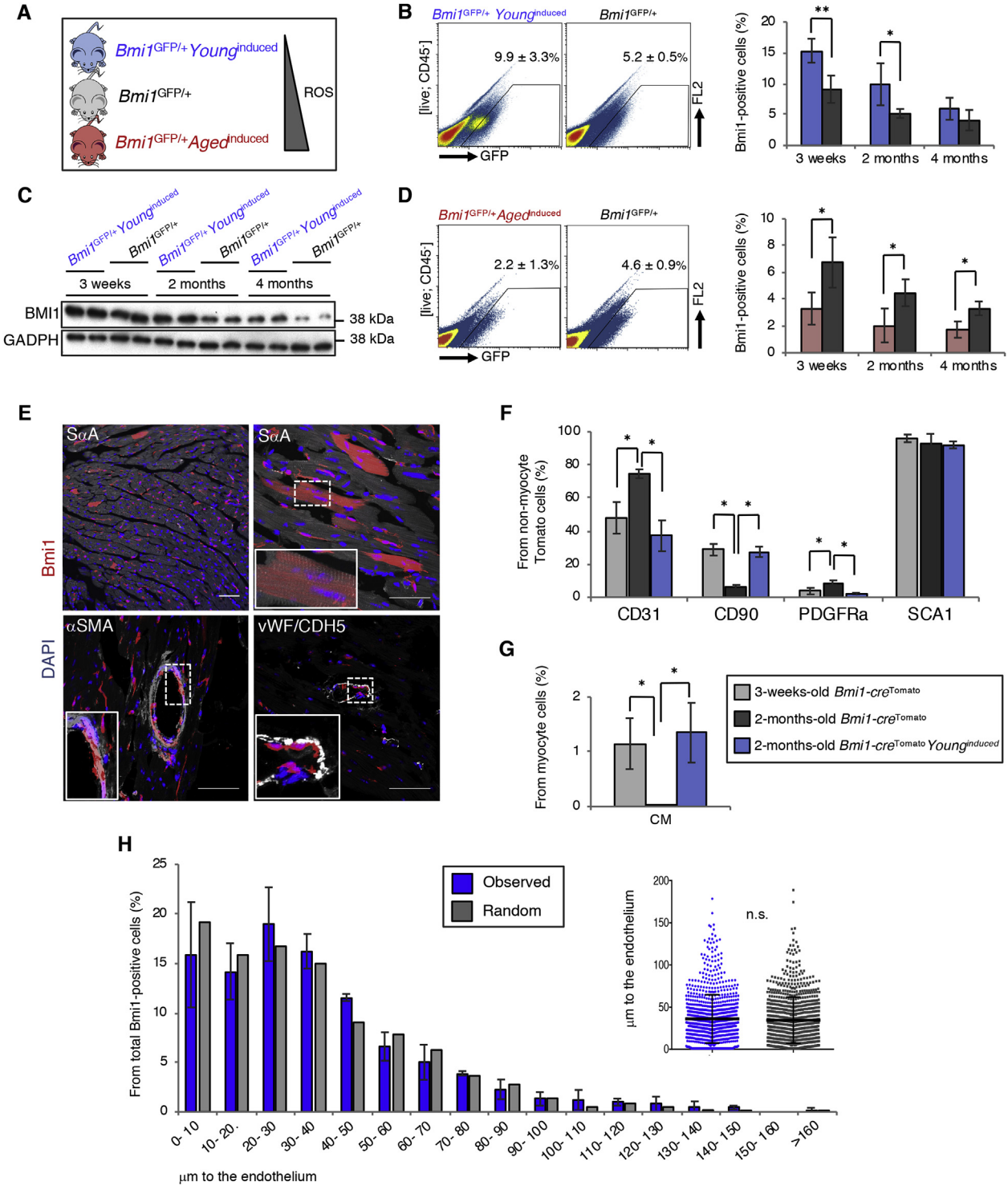

Fig. 5. Genetic ROS modification alters cardiac Bmi1$^+$ DR-cell number, identity and spatial relationship with endothelium. **(A)** Transgenic mouse lines used for rejuvenation (low ROS) and aging (high ROS). **(B)** Representative FACS plots (left) and quantification (right) of GFP$^+$ cardiac cells from Bmi1$^{GFP/+}$Young^{induced} mice and Bmi1$^{GFP/+}$ littermates at indicated ages (n = 8). **(C)** BMI1 expression in whole hearts from Bmi1$^{GFP/+}$Young^{induced} mice and Bmi1$^{GFP/+}$ littermates at indicated ages analyzed by western blot. **(D)** Representative FACS plots (left) and quantification (right) of GFP$^+$ cardiac cells from Bmi1$^{GFP/+}$Aged^{induced} mice and Bmi1$^{GFP/+}$ littermates at indicated ages (n = 8). **(E)** Representative heart cryosections of 2-month-old Bmi1-cre^{Tomato}Young^{induced} mice 5 days post-Tx induction. *Insets*, Bmi1$^+$ cells (2 × magnification). **(F & G)** Comparative FACS characterization of non-myocyte (f) and myocyte (g) cells from 3-week-old (light grey) and 2-month-old (dark grey) Bmi1-cre^{Tomato} mice and 2-month-old Bmi1-cre^{Tomato}Young^{induced} mice (blue) 5 days post-Tx induction (n = 4). **(H)** Distribution of Bmi1$^+$ cells in relation to coronary vasculature (blue) in heart sections from Bmi1-cre^{Tomato}Young^{induced} mice compared with cell distribution of randomly positioned Bmi1$^+$ cells on maps of heart sections in relation to the same cell structure (grey) (n = 4; > 1000 Bmi1$^+$ cells/heart). *Inset*, graph of mean distance. (b,d): *p < 0.05, **p < 0.005; 1-way ANOVA with Tukey post hoc test (f,g) *p < 0.05; Kruskall-Wallis ANOVA test (h): n.s.; 2-sample Kolmogorov-Smirnov test. Bars, 50 µm. Data shown as mean ± SEM.

microenvironment is confined to perivascular positions in an aging-related fashion, suggesting that manipulation of ROS-related pathways and/or stimulation of vascular niche-like structures would constitute an important element in cardiac response to injury.

Conflicts of interest

The authors declare no competing interests.

Funding

DH and GA are FPI predoctoral fellows of the Spanish Ministry of Economy and Competitiveness. This study was supported by grants to AB from the Ministry of Economy and Competitiveness (MINECO/FEDER) (SAF2015-70882-R), Comunidad Autónoma de Madrid (S2011/BMD-2420), Instituto de Salud Carlos III (ISCIII) (RETICS-RD12/0018) and the European Commission (HEALTH-2009_242038) and to SM from the MINECO (SAF2017-83732-R).

Acknowledgements

We thank S Gutierrez from the Confocal Microscopy Unit for computational simulations, MC Moreno and S Escudero for the sorting strategy, I Sánchez and L Domínguez for surgical infarcts, O Klein for the Gli1^{CreERT} mouse line, M Serrano for the G6PD^{Tg} mouse line, J Aragonés and N Fonseca-Balvís for valuable discussion, and K McCreath for editorial assistance.

Appendix A. Supplementary data

Supplementary data to this article can be found online at https://doi.org/10.1016/j.redox.2019.101156.

References

[1] O. Bergmann, S. Zdunek, A. Felker, M. Salehpour, K. Alkass, S. Bernard, ... J. Frisén, Dynamics of cell generation and turnover in the human heart, Cell 161 (7) (2015) 1566–1575, https://doi.org/10.1016/j.cell.2015.05.026.

[2] O. Bergmann, R.D. Bhardwaj, S. Bernard, S. Zdunek, F. Barnabé-Heider, S. Walsh, ... J. Frisén, Evidence for cardiomyocyte renewal in humans, Science 324 (5923) (2009) 98–102, https://doi.org/10.1126/science.1164680.

[3] K. Malliaras, Y. Zhang, J. Seinfeld, G. Galang, E. Tseliou, K. Cheng, ... E. Marbán, Cardiomyocyte proliferation and progenitor cell recruitment underlie therapeutic regeneration after myocardial infarction in the adult mouse heart, EMBO Mol. Med. 5 (2) (2013) 191–209, https://doi.org/10.1002/emmm.201201737.

[4] J.H. van Berlo, O. Kanisicak, M. Maillet, R.J. Vagnozzi, J. Karch, S.C. Lin, ... J.D. Molkentin, c-Kit^{+} cells minimally contribute cardiomyocytes to the heart, Nature 509 (7500) (2014) 337–341, https://doi.org/10.1038/nature13309.

[5] L.E. Neidig, F. Weinberger, N.J. Palpant, J. Mignone, A.M. Martinson, D.W. Sorensen, ... J.H. van Berlo, Evidence for minimal cardiogenic potential of Stem cell antigen 1-positive cells in the adult mouse heart, Circulation 138 (25) (2018) 2960–2962, https://doi.org/10.1161/CIRCULATIONAHA.118.035273.

[6] S. Uchida, P. De Gaspari, S. Kostin, K. Jenniches, A. Kilic, Y. Izumiya, ... T. Braun, Sca1-derived cells are a source of myocardial renewal in the murine adult heart, Stem Cell Rep. 1 (5) (2013) 397–410, https://doi.org/10.1016/j.stemcr.2013.09.004.

[7] W. Kimura, F. Xiao, D.C. Canseco, S. Muralidhar, S. Thet, H.M. Zhang, ... H.A. Sadek, Hypoxia fate mapping identifies cycling cardiomyocytes in the adult heart, Nature 523 (7559) (2015) 226–230, https://doi.org/10.1038/nature14582.

[8] S.E. Senyo, M.L. Steinhauser, C.L. Pizzimenti, V.K. Yang, L. Cai, M. Wang, ... R.T. Lee, Mammalian heart renewal by pre-existing cardiomyocytes, Nature 493 (7432) (2013) 433–436, https://doi.org/10.1038/nature11682.

[9] M. Hesse, M. Doengi, A. Becker, K. Kimura, N. Voeltz, V. Stein, B.K. Fleischmann, Midbody positioning and distance between daughter nuclei enable unequivocal identification of cardiomyocyte cell division in mice, Circ. Res. 123 (9) (2018) 1039–1052, https://doi.org/10.1161/CIRCRESAHA.118.312792.

[10] R. Kramann, R.K. Schneider, D.P. DiRocco, F. Machado, S. Fleig, P.A. Bondzie, ... B.D. Humphreys, Perivascular Gli1^{+} progenitors are key contributors to injury-induced organ fibrosis, Cell Stem Cell 16 (1) (2015) 51–66, https://doi.org/10.1016/j.stem.2014.11.004.

[11] R.J. Vagnozzi, M.A. Sargent, S.J. Lin, N.J. Palpant, C.E. Murry, J.D. Molkentin, Genetic lineage tracing of Sca-1^{+} cells reveals endothelial but not myogenic contribution to the murine heart, Circulation 138 (25) (2018) 2931–2939, https://doi.org/10.1161/CIRCULATIONAHA.118.035210.

[12] D. Herrero, S. Cañón, B. Pelacho, M. Salvador-Bernáldez, S. Aguilar, C. Pogontke, ... A. Bernad, Bmi1-progenitor cell ablation impairs the angiogenic response to myocardial infarction, Arterioscler. Thromb. Vasc. Biol. 38 (2018) 2160–2173, https://doi.org/10.1161/ATVBAHA.118.310778.

[13] S.R. Mekala, P. Wörsdörfer, J. Bauer, O. Stoll, N. Wagner, L. Reeh, ... S. Ergün, Generation of cardiomyocytes from vascular adventitia-resident stem cells, Circ. Res. 123 (6) (2018) 686–699, https://doi.org/10.1161/CIRCRESAHA.117.312526.

[14] L. Dobnikar, A.L. Taylor, J. Chappell, P. Oldach, J.L. Harman, E. Oerton, ... H.F. Jørgensen, Disease-relevant transcriptional signatures identified in individual smooth muscle cells from healthy mouse vessels, Nat. Commun. 9 (1) (2018) 4567, https://doi.org/10.1038/s41467-018-06891-x.

[15] B.C. Du Pré, E.J. Demkes, D.A.M. Feyen, P. Dierickx, S. Crnko, B.J.M. Kok, ... L.W. Van Laake, SCA1^{+} cells from the heart possess a molecular circadian clock and display circadian oscillations in cellular functions, Stem Cell Rep. 9 (3) (2017) 762–769, https://doi.org/10.1016/j.stemcr.2017.07.010.

[16] M. Noseda, M. Harada, S. McSweeney, T. Leja, E. Belian, D.J. Stuckey, ... M.D. Schneider, PDGFRα demarcates the cardiogenic clonogenic Sca1^{+} stem/progenitor cell in adult murine myocardium, Nat. Commun. 6 (2015) 6930, https://doi.org/10.1038/ncomms7930.

[17] I. Valiente-Alandi, C. Albo-Castellanos, D. Herrero, I. Sanchez, A. Bernad, Bmi1^{+} cardiac progenitor cells contribute to myocardial repair following acute injury, Stem Cell Res. Ther. 7 (1) (2016) 100, https://doi.org/10.1186/s13287-016-0355-7.

[18] Z. Chen, W. Zhu, I. Bender, W. Gong, I.Y. Kwak, A. Yellamilli, ... J.H. van Berlo, Pathologic stimulus determines lineage commitment of cardiac c-Kit^{+} cells, Circulation 136 (24) (2017) 2359–2372, https://doi.org/10.1161/CIRCULATIONAHA.117.030137.

[19] S. Banerjee Mustafi, N. Aznar, S.K. Dwivedi, P.K. Chakraborty, R. Basak, P. Mukherjee, ... R. Bhattacharya, Mitochondrial BMI1 maintains bioenergetic homeostasis in cells, FASEB J. 30 (12) (2016) 4042–4055, https://doi.org/10.1096/fj.201600321R.

[20] J.J. Jacobs, K. Kieboom, S. Marino, R.A. DePinho, M. van Lohuizen, The oncogene and Polycomb-group gene Bmi-1 regulates cell proliferation and senescence through the Ink4a locus, Nature 397 (6715) (1999) 164–168, https://doi.org/10.1038/16476.

[21] B. Biehs, J.K. Hu, N.B. Strauli, E. Sangiorgi, H. Jung, R.P. Heber, ... O.D. Klein, BMI1 represses Ink4a/Arf and Hox genes to regulate stem cells in the rodent incisor, Nat. Cell Biol. 15 (7) (2013) 846–852, https://doi.org/10.1038/ncb2766.

[22] J.S. Dovey, S.J. Zacharek, C.F. Kim, J.A. Lees, Bmi1 is critical for lung tumorigenesis and bronchioalveolar stem cell expansion, Proc. Natl. Acad. Sci. U.S.A. 105 (33) (2008) 11857–11862, https://doi.org/10.1073/pnas.0803574105.

[23] Y. Komai, T. Tanaka, Y. Tokuyama, H. Yanai, S. Ohe, T. Omachi, ... H. Ueno, Bmi1 expression in long-term germ stem cells, Sci. Rep. 4 (2014) 6175, https://doi.org/10.1038/srep06175.

[24] E. Sangiorgi, M.R. Capecchi, Bmi1 is expressed *in vivo* in intestinal stem cells, Nat. Genet. 40 (7) (2008) 915–920, https://doi.org/10.1038/ng.165.

[25] Y. Zhou, L. Wang, H.R. Vaseghi, Z. Liu, R. Lu, S. Alimohamadi, ... L. Qian, Bmi1 is a key epigenetic barrier to direct cardiac reprogramming, Cell Stem Cell 18 (3) (2016) 382–395, https://doi.org/10.1016/j.stem.2016.02.003.

[26] D. Herrero, M. Tomé, S. Cañón, F.M. Cruz, R.M. Carmona, E. Fuster, ... A. Bernad, Redox-dependent BMI1 activity drives *in vivo* adult cardiac progenitor cell differentiation, Cell Death Differ. 25 (4) (2018) 807–820, https://doi.org/10.1038/s41418-017-0022-2.

[27] I. Valiente-Alandi, C. Albo-Castellanos, D. Herrero, E. Arza, M. Garcia-Gomez, J.C. Segovia, ... A. Bernad, Cardiac Bmi1^{+} cells contribute to myocardial renewal in the murine adult heart, Stem Cell Res. Ther. 6 (2015) 205, https://doi.org/10.1186/s13287-015-0196-9.

[28] Y. Song, M. Zhao, Y. Xie, T. Zhu, W. Liang, B. Sun, ... Y. Xie, Bmi-1 high-expressing cells enrich cardiac stem/progenitor cells and respond to heart injury, J. Cell Mod. Med. 23 (1) (2019) 104–111, https://doi.org/10.1111/jcmm.13889.

[29] S.J. Morrison, A.C. Spradling, Stem cells and niches: mechanisms that promote stem cell maintenance throughout life, Cell 132 (4) (2008) 598–611, https://doi.org/10.1016/j.cell.2008.01.038.

[30] S. Pinho, T. Marchand, E. Yang, Q. Wei, C. Nerlov, P.S. Frenette, Lineage-biased hematopoietic stem cells are regulated by distinct niches, Dev. Cell 44 (5) (2018) 634–641, https://doi.org/10.1016/j.devcel.2018.01.016.

[31] S.M. Chambers, C.A. Shaw, C. Gatza, C.J. Fisk, L.A. Donehower, M.A. Goodell, Aging hematopoietic stem cells decline in function and exhibit epigenetic dysregulation, PLoS Biol. 5 (8) (2007) e201, https://doi.org/10.1371/journal.pbio.0050201.

[32] J.R. Pineda, M. Daynac, A. Chicheportiche, A. Cebrian-Silla, K. Sii Felice, J.M. Garcia-Verdugo, ... M.A. Mouthon, Vascular-derived TGF-β increases in the stem cell niche and perturbs neurogenesis during aging and following irradiation in the adult mouse brain, EMBO Mol. Med. 5 (4) (2013) 548–562, https://doi.org/10.1002/emmm.201202197.

[33] I.M. Conboy, M.J. Conboy, A.J. Wagers, E.R. Girma, I.L. Weissman, T.A. Rando, Rejuvenation of aged progenitor cells by exposure to a young systemic environment, Nature 433 (7027) (2005) 760–764, https://doi.org/10.1038/nature03260.

[34] S. Nóbrega-Pereira, P.J. Fernandez-Marcos, T. Brioche, M.C. Gomez-Cabrera, A. Salvador-Pascual, J.M. Flores, ... M. Serrano, G6PD protects from oxidative damage and improves healthspan in mice, Nat. Commun. 7 (2016) 10894, https://doi.org/10.1038/ncomms10894.

[35] L.M. Carlsson, J. Jonsson, T. Edlund, S.L. Marklund, Mice lacking extracellular superoxide dismutase are more sensitive to hyperoxia, Proc. Natl. Acad. Sci. U.S.A. 92 (14) (1995) 6264–6268.

[36] L.R. Miller, C. Marks, J.B. Becker, P.D. Hurn, W.J. Chen, T. Woodruff, J.A. Clayton, Considering sex as a biological variable in preclinical research, FASEB J. 31 (1)

(2017) 29–34, https://doi.org/10.1096/fj.201600781R.
[37] K. Ashina, Y. Tsubosaka, T. Nakamura, K. Omori, K. Kobayashi, M. Hori, ... T. Murata, Histamine induces vascular hyperpermeability by increasing blood flow and endothelial barrier disruption *in vivo*, PLoS One 10 (7) (2015) e0132367, , https://doi.org/10.1371/journal.pone.013236.
[38] C.W. Sharp, A. Ottolenghi, H.S. Posner, Correlation of paraquat toxicity with tissue concentrations and weight loss of the rat, Toxicol. Appl. Pharmacol. 22 (2) (1972) 241–251.
[39] Q.G. Dong, S. Bernasconi, S. Lostaglio, R.W. De Calmanovici, I. Martin-Padura, F. Breviario, ... A. Vecchi, A general strategy for isolation of endothelial cells from murine tissues. Characterization of two endothelial cell lines from the murine lung and subcutaneous sponge implants, Arterioscler. Thromb. Vasc. Biol. 17 (8) (1997) 1599–1604.
[40] S. Parrinello, I. Napoli, S. Ribeiro, P. Wingfield Digby, M. Fedorova, D.B. Parkinson, ... A.C. Lloyd, EphB signaling directs peripheral nerve regeneration through Sox2-dependent Schwann cell sorting, Cell 143 (1) (2010) 145–155, https://doi.org/10.1016/j.cell.2010.08.039.
[41] N. Hosen, T. Yamane, M. Muijtjens, K. Pham, M.F. Clarke, I.L. Weissman, Bmi-1-green fluorescent protein-knock-in mice reveal the dynamic regulation of Bmi-1 expression in normal and leukemic hematopoietic cells, Stem Cell. 25 (7) (2007) 1635–1644, https://doi.org/10.1634/stemcells.2006-0229.
[42] M. Ushio-Fukai, J. Rehman, Redox and metabolic regulation of stem/progenitor cells and their niche, Antioxidants Redox Signal. 21 (11) (2014) 1587–1590, https://doi.org/10.1089/ars.2014.5931.
[43] Y. Kunisaki, I. Bruns, C. Scheiermann, J. Ahmed, S. Pinho, D. Zhang, ... P.S. Frenette, Arteriolar niches maintain haematopoietic stem cell quiescence, Nature 502 (7473) (2013) 637–643, https://doi.org/10.1038/nature12612.
[44] C. Ottone, B. Krusche, A. Whitby, M. Clements, G. Quadrato, M.E. Pitulescu, ... S. Parrinello, Direct cell-cell contact with the vascular niche maintains quiescent neural stem cells, Nat. Cell Biol. 16 (11) (2014) 1045–1056, https://doi.org/10.1038/ncb3045.
[45] M.D. Muzumdar, B. Tasic, K. Miyamichi, L. Li, L. Luo, A global double-fluorescent Cre reporter mouse, Genesis 45 (9) (2007) 593–605, https://doi.org/10.1002/dvg.20335.
[46] K. Jang, M. Kim, C.A. Gilbert, F. Simpkins, T.A. Ince, J.M. Slingerland, VEGFA activates an epigenetic pathway upregulating ovarian cancer-initiating cells, EMBO Mol. Med. 9 (3) (2017) 304–318, https://doi.org/10.15252/emmm.201606840.
[47] H.U. Wang, Z.F. Chen, D.J. Anderson, Molecular distinction and angiogenic interaction between embryonic arteries and veins revealed by ephrin-B2 and its receptor Eph-B4, Cell 93 (5) (1998) 741–753.
[48] A. Di Lorenzo, C. Fernández-Hernando, G. Cirino, W.C. Sessa, Akt1 is critical for acute inflammation and histamine-mediated vascular leakage, Proc. Natl. Acad. Sci. U.S.A. 106 (34) (2009) 14552–14557, https://doi.org/10.1073/pnas.0904073106.
[49] J.A. Spencer, F. Ferraro, E. Roussakis, A. Klein, J. Wu, J.M. Runnels, ... C.P. Lin, Direct measurement of local oxygen concentration in the bone marrow of live animals, Nature 508 (7495) (2014) 269–273, https://doi.org/10.1038/nature13034.
[50] J.J. Chong, V. Chandrakanthan, M. Xaymardan, N.S. Asli, J. Li, I. Ahmed, ... R.P. Harvey, Adult cardiac-resident MSC-like stem cells with a proepicardial origin, Cell Stem Cell 9 (6) (2011) 527–540, https://doi.org/10.1016/j.stem.2011.10.002.
[51] F. Kocabas, A.I. Mahmoud, D. Sosic, E.R. Porrello, R. Chen, J.A. Garcia, ... H.A. Sadek, The hypoxic epicardial and subepicardial microenvironment, J. Cardiovasc. Transl. Res. 5 (5) (2012) 654–665, https://doi.org/10.1007/s12265-012-9366-7.
[52] B.A. Fioret, J.D. Heimfeld, D.T. Paik, A.K. Hatzopoulos, Endothelial cells contribute to generation of adult ventricular myocytes during cardiac homeostasis, Cell Rep. 8 (1) (2014) 229–241, https://doi.org/10.1016/j.celrep.2014.06.004.
[53] Q. Chen, H. Zhang, Y. Liu, S. Adams, H. Eilken, M. Stehling, ... R.H. Adams, Endothelial cells are progenitors of cardiac pericytes and vascular smooth muscle cells, Nat. Commun. 7 (2016) 12422, https://doi.org/10.1038/ncomms12422.
[54] E.M. Zeisberg, O. Tarnavski, M. Zeisberg, A.L. Dorfman, J.R. McMullen, E. Gustafsson, ... R. Kalluri, Endothelial-to-mesenchymal transition contributes to cardiac fibrosis, Nat. Med. 13 (8) (2007) 952–961, https://doi.org/10.1038/nm1613.
[55] S.J. Kattman, T.L. Huber, G.M. Keller, Multipotent Flk-1 $^{+}$ cardiovascular progenitor cells give rise to the cardiomyocyte, endothelial, and vascular smooth muscle lineages, Dev. Cell 11 (5) (2006) 723–732, https://doi.org/10.1016/j.devcel.2006.10.002.
[56] A.J. Putnam, The instructive role of the vasculature in stem cell niches, Biomater. Sci. 2 (11) (2014) 1562–1573, https://doi.org/10.1039/C4BM00200H.
[57] B.N. Puente, W. Kimura, S.A. Muralidhar, J. Moon, J.F. Amatruda, K.L. Phelps, ... H.A. Sadek, The oxygen-rich postnatal environment induces cardiomyocyte cell-cycle arrest through DNA damage response, Cell 157 (3) (2014) 565–579, https://doi.org/10.1016/j.cell.2014.03.032.
[58] F.L. Crespo, V.R. Sobrado, L. Gomez, A.M. Cervera, K.J. McCreath, Mitochondrial reactive oxygen species mediate cardiomyocyte formation from embryonic stem cells in high glucose, Stem Cell. 28 (7) (2010) 1132–1142, https://doi.org/10.1002/stem.441.
[59] S. Judge, Y.M. Jang, A. Smith, T. Hagen, C. Leeuwenburgh, Age-associated increases in oxidative stress and antioxidant enzyme activities in cardiac interfibrillar mitochondria: implications for the mitochondrial theory of aging, FASEB J. 19 (3) (2005) 419–421, https://doi.org/10.1096/fj.04-2622fje.
[60] D.F. Dai, L.F. Santana, M. Vermulst, D.M. Tomazela, M.J. Emond, M.J. MacCoss, ... P.S. Rabinovitch, Overexpression of catalase targeted to mitochondria attenuates murine cardiac aging, Circulation 119 (21) (2009) 2789–2797, https://doi.org/10.1161/CIRCULATIONAHA.108.822403.
[61] R. Wessells, E. Fitzgerald, N. Piazza, K. Ocorr, S. Morley, C. Davies, ... R. Bodmer, d4eBP acts downstream of both dTOR and dFoxo to modulate cardiac functional aging in drosophila, Aging Cell 8 (5) (2009) 542–552, https://doi.org/10.1111/j.1474-9726.2009.00504.x.
[62] S.E. Schriner, N.J. Linford, G.M. Martin, P. Treuting, C.E. Ogburn, M. Emond, ... P.S. Rabinovitch, Extension of murine life span by overexpression of catalase targeted to mitochondria, Science 308 (5730) (2005) 1909–1911, https://doi.org/10.1126/science.1106653.
[63] Y.A. Chiao, S.C. Kolwicz, N. Basisty, A. Gagnidze, J. Zhang, H. Gu, ... P.S. Rabinovitch, Rapamycin transiently induces mitochondrial remodeling to reprogram energy metabolism in old hearts, Aging 8 (2) (2016) 314–327, https://doi.org/10.18632/aging.100881.